AAS 13-264

MULTI-OBJECTIVE OPTIMISATION OF MANY-REVOLUTION, LOW-THRUST ORBIT RAISING FOR DESTINY MISSION

Federico Zuiani[*], Yasuhiro Kawakatsu[†] and Massimiliano Vasile[‡]

This work will present a Multi-Objective approach to the design of the initial, Low-Thrust orbit raising phase for JAXA's proposed technology demonstrator mission DESTINY. The proposed approach includes a simplified model for Low Thrust, many-revolution transfers, based on an analytical orbital averaging technique, and a simplified control parameterisation. Eclipses and J_2 perturbation are also accounted for. This is combined with a stochastic optimisation algorithm to solve optimisation problems in which conflicting performance figures of DESTINY's trajectory design are concurrently optimised. It will be shown that the proposed approach provides for a good preliminary investigation of the launch window and helps identifying critical issues to be addressed in future design phases.

INTRODUCTION

The Demonstration and Experiment for Space Technology and INterplanetary voYage (DESTINY)[1] is a technology demonstrator mission which is currently being developed as a candidate third mission of ISAS/JAXA's small science satellite series. Its main objective is that of gaining flight heritage for a number of novel technologies, which include, among others, the new μ20 Ion engine, the new Epsilon launch vehicle, ultra-lightweight solar panels and an advanced thermal control. In addition, it will also provide a test-bed for new techniques for Low Thrust (LT), interplanetary mission design and operation.

The proposed mission profile for DESTINY, as shown in Figure 1, envisions:

1) Injection into an inclined elliptical orbit (with semi-major axis around 20000 km) by means of the Epsilon rocket.
2) Spiralling phase in which the μ20 engine will raise the orbit in order to encounter the Moon.
3) Lunar swing-by.
4) Injection into a Halo orbit at the Sun-Earth L_2 Point.
5) Additionally, if possible, a final escape from L_2 is also desirable.

[*] Ph.D. Candidate, School of Engineering, University of Glasgow, James Watt South Building, Glasgow G12 8QQ, United Kingdom. E-mail: f.zuiani.1@research.gla.ac.uk. Currently at ISAS/JAXA as JSPS Fellow.
[†] Associate Professor, Institute of Space and Astronautical Science, Japan Aerospace Exploration Agency, 3-1-1 Yoshino-dai, Chuo-ku, Sagamihara-shi, Kanagawa-ken, 252-5210, Japan. E-mail: kawakatsu.yasuhiro@jaxa.jp
[‡] Reader, Department of Mechanical and Aerospace Engineering, University of Strathclyde, Graham Hills Building, 50 George Street, Glasgow G1 1QE, United Kingdom. E-mail: massimiliano.vasile@strath.ac.uk

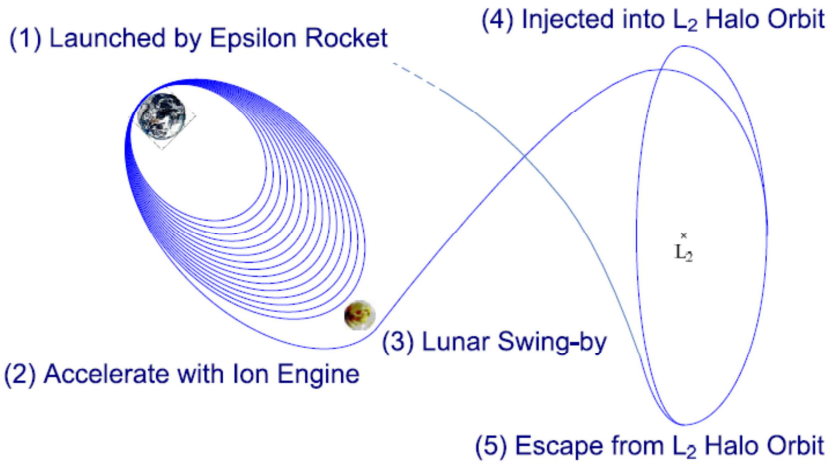

Figure 1. DESTINY preliminary mission profile.

The early LT orbit raising phase presents an interesting mission design challenge, since a many trade-offs are to be made between different performance figures; at the same time, technological limitations from bus design impose a number of constraints on trajectory design. In particular, the time to reach the Moon encounter is upper bounded at 1.5 years but shorter transfer times might also be advantageous. On the other hand, in the latter case, the required ΔV is likely to be higher; while this, given the available fuel and the high efficiency of the μ20 engine, will not prevent reaching the Halo orbit, it will possibly affect the feasibility of the optional post-Halo escape phase. It should also be noted that, during the orbit raising phase the spacecraft will spend a long period of time within the highly radiative environment of the Van Allen belts. This time should be minimised in order to reduce the total radiation dose and therefore the mass of the required shielding for electronic components. Similarly, eclipse duration during the transfer, influences both trajectory design, since engine operation has to be interrupted while in shadow, and spacecraft bus design because it imposes constraints on battery sizing. Finally the conditions, in terms of orbit geometry, with which the Moon is encountered, also require trade-off analysis, since they are strongly linked with the trajectory design of the following phase which will lead DESTINY spacecraft to the designated L_2 Halo orbit.

The presence of many conflicting requirements will be tackled in this work by adopting a Multi-Objective (MO) design approach, in which multiple performance figures are concurrently optimised. Multi-objective design of Low-Thrust trajectories is a challenging optimisation problem and the reasons for this are twofold: first, the computation of a single LT transfer is already a complex problem because it generally requires the solution of a Low-Thrust, Two Point, Boundary Value Problem (LT-2PBVP), and given the complex dynamics involved and the potentially large number of control parameters this is usually computationally very expensive. Secondly, the solution of multi-objective optimisation problems is usually accomplished by means of global multi-objective stochastic algorithms which require the evaluation of a large number of candidate solutions in order to find a set of Pareto optimal ones. This fact makes the application of traditional LT trajectory design techniques computationally unfeasible. Therefore, in this work a novel approach will be proposed, which combines an analytical averaging technique with a simplified parameterisation of the thrust control. The former is meant at considerably lowering the computational time needed to propagate long spiralling trajectories, like the one of DESTINY, while the latter is aimed at reducing the number of parameters which define the thrusting strategy. This al-

lows combining the proposed analytical averaged approach with a MO optimisation algorithm[2] in order to solve a complex MO problem in which hundreds of thousands candidate solutions are evaluated.

LOW THRUST, MANY-REVOLUTION TRANSFERS

In past works, other authors have already proposed approaches to the design of low thrust, many-revolution transfers. Among them, there is a good number of methods based on analytical solutions of the equations of motion, for example under the assumption of small eccentricity[3,4,5]; averaging techniques[6,7] have also been combined direct transcription optimisation techniques. However, most of these proposals lack flexibility for treating generic many-revolution transfer problems. Adding to this, Multi-Objective LT transfer optimisation is a field which is still in its infancy.

In the proposed approach, the motion of the spacecraft is propagated by means of an orbital averaging technique, in which the net variation of the orbital elements along a single revolution is computed; then this averaged over the orbit period and the resulting quantity is integrated numerically over the long time periods. In particular the variation of orbital elements $\Delta\mathbf{E}_{2\pi}$ along a single revolution due to the thrust is computed by means of an analytical, first-order solution of perturbed Keplerian motion[8,9,10], which has shown to guarantee adequate accuracy at a lower computational cost compared to numerical integration. The contribution of the J_2 perturbation is also included. An extensive description of the analytical formulae and of their accuracy can be found in[8,9,10] and will not be repeated here in detail for the sake of conciseness.

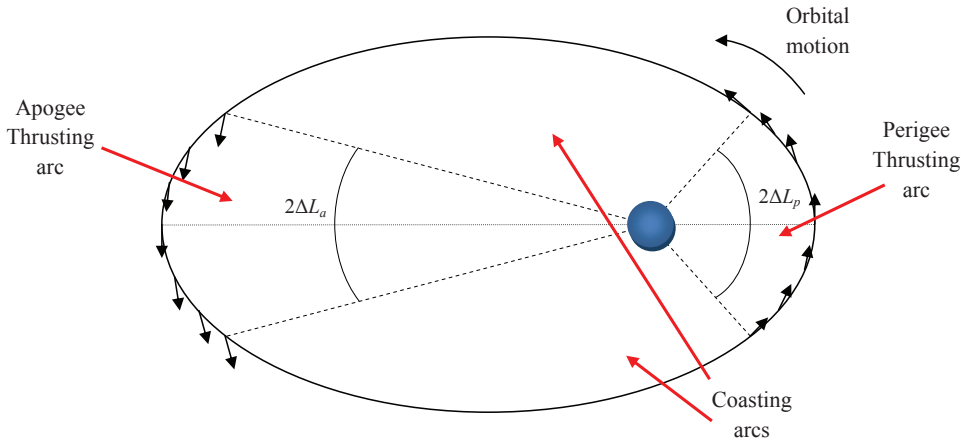

Figure 2. Thrusting pattern.

In order to keep the number of parameters low, a number of assumptions on the thrusting strategy are introduced. First of all, an on/off control is assumed, in the sense that at a given instant, the thrust magnitude can be either zero or the maximum value permitted by engine specifications. Secondly, it is assumed that the thrust direction is purely in plane and directed along the tangential direction, which maximises the instantaneous variation of orbital energy. Thus, one has to define the timing of the thrust switching. The control parameterisation is similar to the one proposed in[11], in which each revolution is divided in 4 sectors, as shown in Figure 2: a Perigee thrusting arc, an Apogee thrusting arc and two coasting arcs in between. The first, of amplitude ΔL_p, is meant ideally to alter apocenter altitude by thrusting in either way along the tangential di-

rection. Similarly, the second alters the pericenter altitude by thrusting tangentially around the apoapsis for an arc of amplitude ΔL_a. The variation of the orbital elements along the thrusting arcs is computed with the analytical formulae. If a plane change were also required, an out-of-plane component described by elevation β_p and β_a, could also have been introduced, but this is not done here. Therefore, the amplitudes of the arcs ΔL_p and ΔL_a are the quantities to be set to define a control profile.

Given the above mentioned control profile, the propagation of the equations of motion is performed by means of an averaging technique:

$$\begin{aligned} \mathbf{E}(t) &= \mathbf{E}_0 + \int_{t_0}^{t} \dot{\mathbf{E}}_{avg}\left(\tau, \mathbf{E}(\tau), \overline{\Delta L}_p(\tau), \overline{\Delta L}_a(\tau)\right) d\tau \\ \dot{\mathbf{E}}_{avg} &= \frac{\Delta \mathbf{E}_{2\pi}}{T_{2\pi}} \end{aligned} \tag{1}$$

where $\Delta\mathbf{E}_{2\pi}$ is the variation of the orbital elements computed by propagating the discontinuous control profile, as described in the previous section, over an arc of 2π. $T_{2\pi}$ is the orbital period associated to this arc. As already mentioned, this propagation over 2π is performed analytically, while the averaged variation $\dot{\mathbf{E}}_{avg}$ is propagated with a Runge-Kutta integration method.

The terms $\overline{\Delta L}_p$ and $\overline{\Delta L}_a$ are defined as a piecewise linear interpolation with respect to time, from n_{nodes} nodal values, uniformly spaced within the integration boundaries. For example, in the case of $\overline{\Delta L}_p$, one can write:

$$\overline{\Delta L}_p(t) = f_{interp}\left(\mathbf{t}, \Delta\mathbf{L}_p, t\right) \tag{2}$$

where $\Delta\mathbf{L}_p$ is a vector containing the n_{nodes} nodal values, $\mathbf{t}$ is the vector which collects the corresponding times at which the nodal values are specified. f_{interp} defines a piecewise linear interpolation.

In previous works[9,10], it has been shown that this technique allows for a fast propagation of long, many-revolution, Low-Thrust transfers, while maintaining adequate accuracy. However, an obvious drawback is that, since the propagation of the motion is performed by averaging, all instantaneous information, like for example the actual position of the spacecraft along an orbit, is lost. However, for the purposes of the present preliminary analysis, this is a secondary concern and the averaged propagation is deemed as adequate in computing the figures of merit required by the Multi-Objective optimisation process.

Eclipse modelling

As already mentioned, one of the tasks of this study is that of minimising the maximum eclipse encountered by DESTINY during the orbit raising phase. At the same time, constraints on power generation require the interruption of engine operation while the spacecraft is in shadow. In this sense, with reference to Figure 2, along a given orbit, it is necessary to compute the eclipse entry and exit points in order to modify the thrusting strategy accordingly. In this work, a cylindrical model for Earth's shadow is adopted (see Figure 3), which is deemed as adequate in the case of a spacecraft in Earth orbit. In order to identify the eclipse entry and exit points one has to find the true anomalies of the geometrical intersections between the cylinder and the osculating

orbit. The mathematical formulation of this problem can be found in[12,13] and will not be repeated here. Starting from the Osculating Orbital elements and the current Sun-Earth vector, this formulation leads to a quartic equation in $cos\theta$, which can be solved either analytically by means of Ferrari's method, as is done in this work, or numerically with a root-finding algorithm. Note that out of the 4 roots of the quartic polynomial, two are spurious.

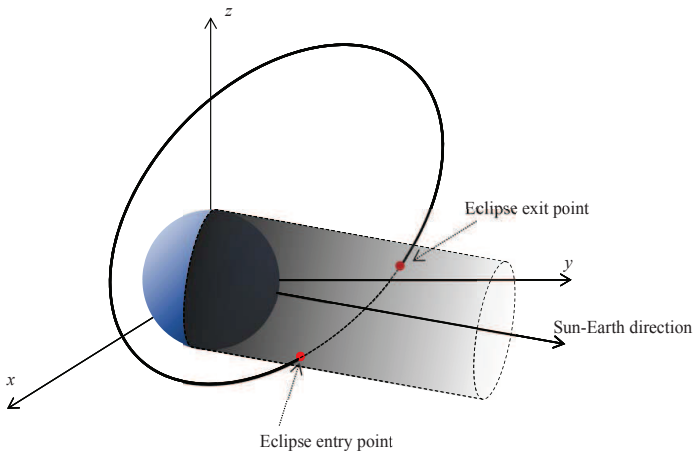

Figure 3. Shadow model.

Once the shadow entry and exit points are known, one can correct the thrusting and coasting arcs as shown in Figure 4. Apart from identifying the shadow regions, this formulation also allows one to analytically compute the duration t_{ecl} of the eclipse itself, and thus from this the duration of the maximum eclipse $t_{ecl,max}$ can be easily estimated.

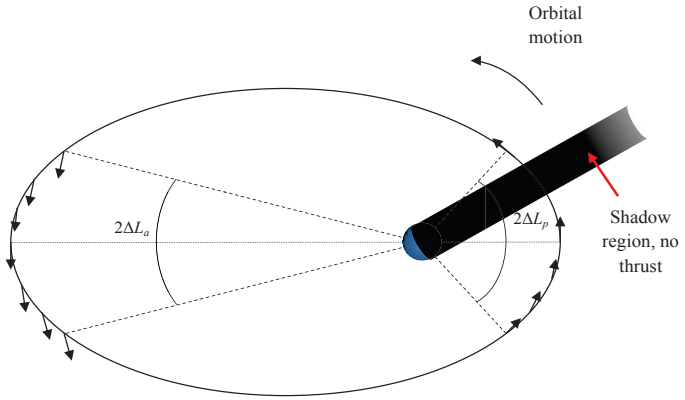

Figure 4. Thrust pattern with eclipse region.

Note however, that this model is valid under the assumption that the relative position of the shadow region with respect to the orbit plane will not change considerably during an orbital revolution. In other words, the shadow region is assumed to be "frozen" along a single revolution. Given the typical time frame of the Sun's dynamics, this assumption is perfectly valid when the orbital period is comparatively small, roughly up to a few days. For larger orbits, what happens is that the orbital period becomes of the same order of magnitude of the time which takes the orbit plane to cross the shadow region. In this sense, during an orbital period the portion of orbit in shadow changes considerably, and thus the "frozen" model proposed here is no longer applicable.

At the same time, however, it also means that there will be just a single eclipse in that revolution and not a sequence of eclipses in close succession as it happens when the orbital period is small. Therefore, it can be assumed that with proper phasing correction at some point before this single eclipse, the latter can be shortened or even avoided altogether. For this reason, it is decided here to ignore these isolated eclipses, in the computation of the maximum eclipse duration, since eclipse avoidance strategies can be easily implemented at a later, more detailed design stage.

DESTINY TRAJECTORY MODEL

The purpose of this study is that of optimising the strategy for DESTINY's orbit raising phase in order to concurrently minimise four figures of merit: the time of flight *ToF*, the total Ion Engine System operation time *IES*, the time spent within the radiation belt t_{belt} and finally the duration of the maximum eclipse encountered $t_{ecl,max}$. The latter, in addition, is to be kept below 1 h, due to constraints on battery size. The maximum time of flight allowed for the orbit raising phase is 550 days, i.e. about 1.5 years.

As a result of the inputs from the design team of the Epsilon Launch Vehicle, the initial orbit parameters after release from the launcher are assumed to be those reported in Table 1.

Table 1. DESTINY initial orbit parameters in the J2000 Earth Fixed reference frame.

a (km)	e	i	Ω	ω	M
20953	0.69	32°	21°	124°	5°

Note that, the initial orbital elements are specified with respect to the J2000 Earth Fixed reference frame, i.e. a moving frame, and thus the actual value of Ω in the inertial reference frame is dependent on the launch epoch. After release from the launcher, a 30-day commissioning phase is imposed, in which the spacecraft is not allowed to perform any manoeuver.

The terminal condition to be reached at the end of the orbit phase is a radius of 300000 km at the intersection between the orbit and the current lunar orbital plane. This condition reflects the fact that at this preliminary stage it has been decided to uncouple the design of the orbit raising phase from that of the Lunar encounter and subsequent interplanetary phase. Note also that, given the relative angle between the lunar orbit plane and DESTINY's, the intersection between the two might occur quite far from DESTINY's apoapsis and therefore the latter might be much higher than 300000 km.

The preliminary specifications for DESTINY spacecraft are reported in Table 2.

Table 2. DESTINY spacecraft characteristics.

Initial mass (kg)	Engine thrust (mN)	Specific impulse (s)
400	40	3800

The powerful μ 20 engine, mounted on a small spacecraft, produces a relatively high acceleration of 10^{-4} m/s^2. At the same time, the high specific impulse of this ion engine ensures good propellant efficiency.

The design parameters which are to be optimised are the departure epoch and the parameters of the thrust vector. For each candidate set for these parameters, the propagation technique presented in the previous section is used to propagate the orbital until the terminal condition of 300000 km radius on the lunar orbit plane has been verified, or else when the maximum time of flight allowed, 550 days, has been reached. From this it is possible to compute the total time of flight *ToF*, total engine operation time *IES*, the time within the radiation belt t_{belt} and the duration of the maximum longest eclipse $t_{ecl,max}$. Note that, t_{belt} is defined simply as the time for which the spacecraft is below 20000 km altitude. The candidate parameter sets will be generated by means of a Multi-Objective optimisation algorithm.

MULTI-OBJECTIVE OPTIMISATION OF DESTINY'S ORBIT RAISING

The design of DESTINY's orbit raising phase can be formulated as a Multi-Objective optimisation problem in the form:

$$\min_{\mathbf{x}\in D} \mathbf{f}\left(\mathbf{x}\right) \tag{3}$$

where **f** is the vector of the objectives:

$$\mathbf{f} = \left[ToF \quad IES \quad t_{belt} \quad t_{ecl,max} \right] \tag{4}$$

x is the parameter vector and *D* is its domain. **x** comprises the departure epoch, decomposed as *date* in MJD2000 and *time* and the semi-aplitudes of the perigee and apogee thrusting arcs, expressed as the values of ΔL_p and ΔL_a at 8 reference nodes, as in Eq. (2). Note that *date* is meant as the integer part of the number of days since epoch -0.5 MJD2000, while *time* is intended as the number of hours since the midnight of the day defined by *date*.

$$\mathbf{x} = \left[date \quad time \quad \cdots \quad \Delta L_{p,i} \quad \cdots \quad \Delta L_{a,i} \quad \cdots \right] \quad i = 1,...,8 \tag{5}$$

The reason, for which the departure epoch is here expressed as day and hour, is that preliminary tests revealed that the objective functions showed wide oscillations with respect to the departure epoch and that the two scales of these oscillations were of the magnitude of a day and a year. This is related to the orientation of the initial orbital plane with respect to the Ecliptic plane and the lunar plane. Since, as mentioned earlier, the initial orbital elements in Table 1 are defined as relative to the Earth, i.e. a rotating reference frame, it follows that Ω in the Equatorial inertial reference frame experiences a short term evolution due to the Earth's rotation around its axis, superimposed to a long term variation due to the Earth's motion in the solar system (plus other secular perturbations). Therefore, by decomposing the departure epoch into *date* and *time*, one is able to decouple these two dynamics. The boundaries for the domain *D* are reported in Table 3.

Table 3. Boundaries for optimisation parameters.

Variable	*date* (d)	*time* (h)	$\Delta L_{p,i}$ (°)	$\Delta L_{a,i}$ (°)
Lower bound	0	0	0	0
Upper bound	365	24	180	180

In summary, each transfer is described by a total of 18 optimisation parameters. Regarding the performance parameters in the vector **f**, as already mentioned there are four figures of merit which are to be concurrently minised, *ToF*, *IES*, t_{belt} and $t_{ecl,max}$, which would translate into a 4-objective optimisation problem. In the following sub-section, it is decided to solve a reduced 3-

objective problem first, without $t_{ecl,max}$ as an objective or constraint. This is done because, generally speaking, a 3-objective problem is easier to visualise and analyse. It will also show how the solution set changes, when the fourth objective will be re-introduced and the full optimisation problem solved. In both cases the Multi-Objective optimisation problem in Eq. (3) is solved with MACS2, a hybrid-memetic optimisation algorithm designed by the authors[14,15].

3-Objective problem

For this 3-objective problem, MACS2 is set to run for a maximum of $3 \cdot 10^5$ function evaluations. Population size is set at 150 individuals, of which 30 perform social actions.

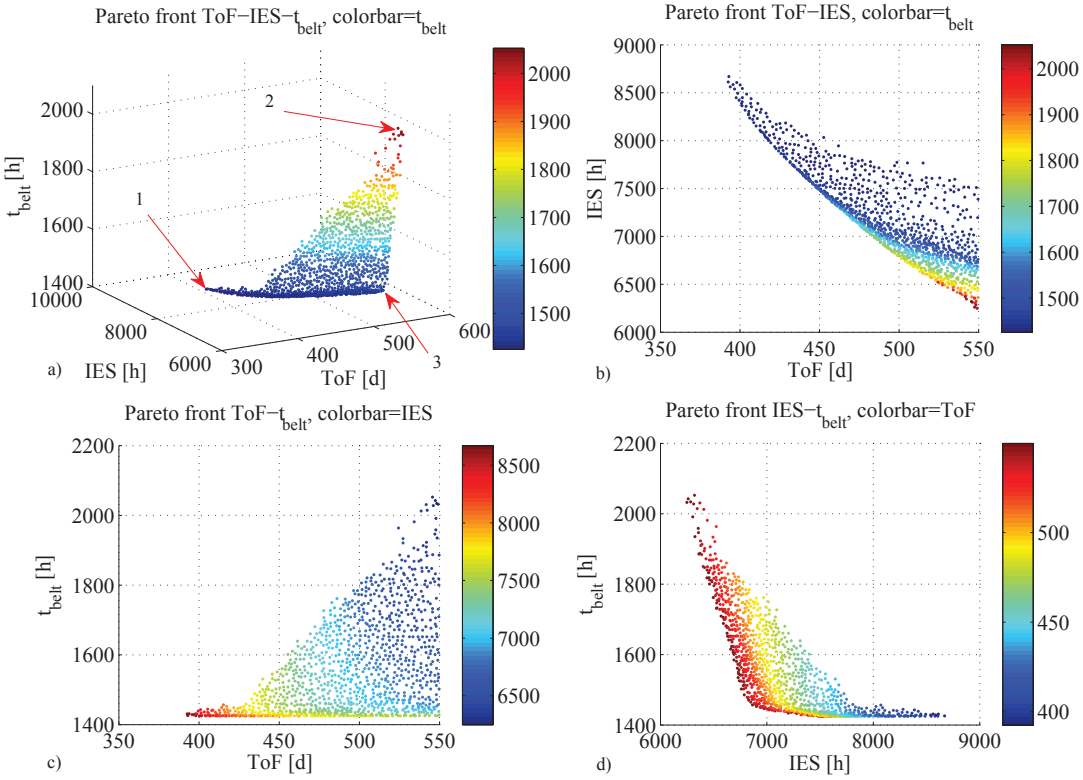

Figure 5. 3-Objective problem: a) Pareto front. Projections on the b) *ToF-IES* c) *ToF-*t_{belt} d) *IES-*t_{belt} sub-spaces.

Figure 5a shows the optimal objective set. For more clarity, Figure 5b-c-d show their projections on the bi-dimensional subspaces. By examining the extreme points for each objective, one can see that, for example, the minimum transfer time is around 400 days, which requires a total of 8600 hours of engine operations. On the other hand, the minimum IES solution requires around 6300 hours for a 550 days transfer. Similarly, the minimum time spent in the radiation belt is above 1400 hours. The *ToF-IES* projection in Figure 5b shows the typical pattern of propellant versus transfer time trade-off. This implies that any reduction in propellant consumption is paid for by an increase in transfer time and vice-versa. It is also interesting to note from Figure 5d that, in a similar way, any reduction in propellant consumption below 7300 hours invariably requires an increase in t_{belt}. Moreover, the minimum *ToF* solution is also a minimiser for t_{belt}. The reasons for this will be explained later in this section. Figure 6 shows the distribution of the optimal solutions along the launch window and shows that they are aligned along a diagonal line in the date-time space. As mentioned earlier, date and time are determining the initial Ω in the Equatorial

reference frame. Given the relative inclination between the Equator and the lunar orbit plane, this parameter consequently affects the elevation of the apsis direction w.r.t. the lunar orbit plane. Since the termination condition is defined at the intersection with this plane, the higher the elevation is, the higher the final semi-major axis will have to be and therefore the longer or the more expensive the transfer will be. Therefore, the optimal solutions line on the diagonal line which corresponds to the initial Ω which gives the lowest elevation of the line of apsis on the lunar orbit plane at the end of the transfer.

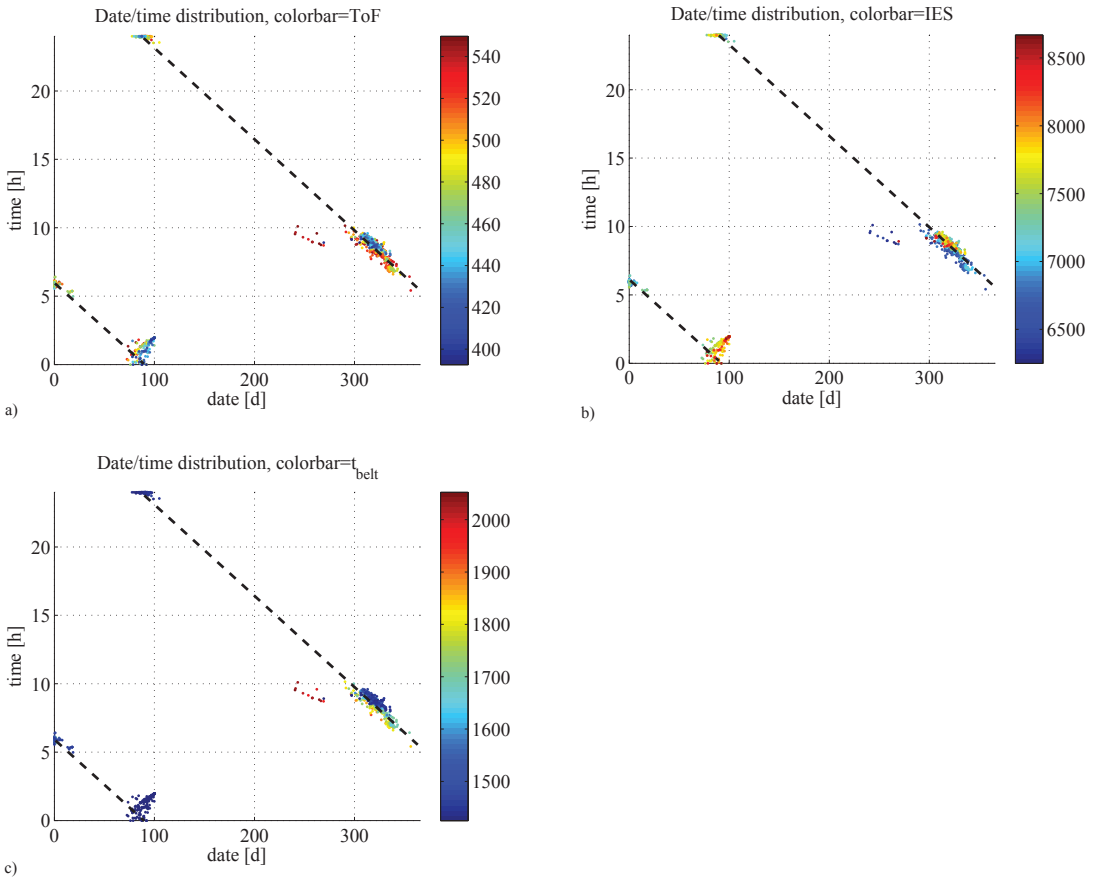

Figure 6. 3-Objective problem: distribution of the optimal solutions w.r.t. the departure date: a) *ToF* b) *IES* c) t_{belt}.

From Figure 5a one can identify three different classes of solutions: those which minimise time of flight and time in the radiation belt (1); those which minimise propellant cost (2); and finally, those which minimise t_{belt} but at the same time also somewhat minimise *IES* by allowing for the maximum *ToF* of 550 days (3).

Table 4 reports a comparison of the three solution types. As one can see solution 1 has the lowest time of flight, 392 days and at the same time also the lowest time spent within the radiation belt, 1431 hours. On the other hand, ion engine operation time is the highest, at 8632 hours. The opposite applies to the second solution, with an engine operation time of just 6349 hours but with the highest admissible time of flight of 550 days and a high t_{belt} of over 2000 hours. The third case is very interesting, for the reason that it has the minimum t_{belt} like the first one, but at

the same time its fuel consumption is not as high as the first case, since the time of flight has been allowed to increase up to almost 550 days.

Table 4. Summary of sample solutions

	Type	*date* (d)	*time* (h)	*ToF* (d)	*IES* (h)	t_{belt} (h)
1	min(*ToF*)	295	9.2	392	8632	1431
2	min(*IES*)	266	8.7	550	6249	2032
3	min(t_{belt}),max(*ToF*)	329	8.3	550	6865	1457

In order to better understand the differences between the three cases, Figure 7, Figure 9 and Figure 11 show the thrusting arc length and the time history of the perigee/apogee radii for each of them. From Figure 7a one can see that the semi-amplitude of the thrusting arc for the minimum *ToF* case is always 180 degrees (except for the initial commissioning phase), which translates into a continuous thrust profile. And as Figure 7b shows, perigee and apogee are concurrently raised, with a monotonic decrease of the eccentricity, which reaches 0.2 at the end of the transfer. Note also that the Apogee is around 300000 km when the terminal condition is reached, which confirms what said earlier that the optimal solutions reach the terminal condition with the line of apses lying on the lunar orbital plane.

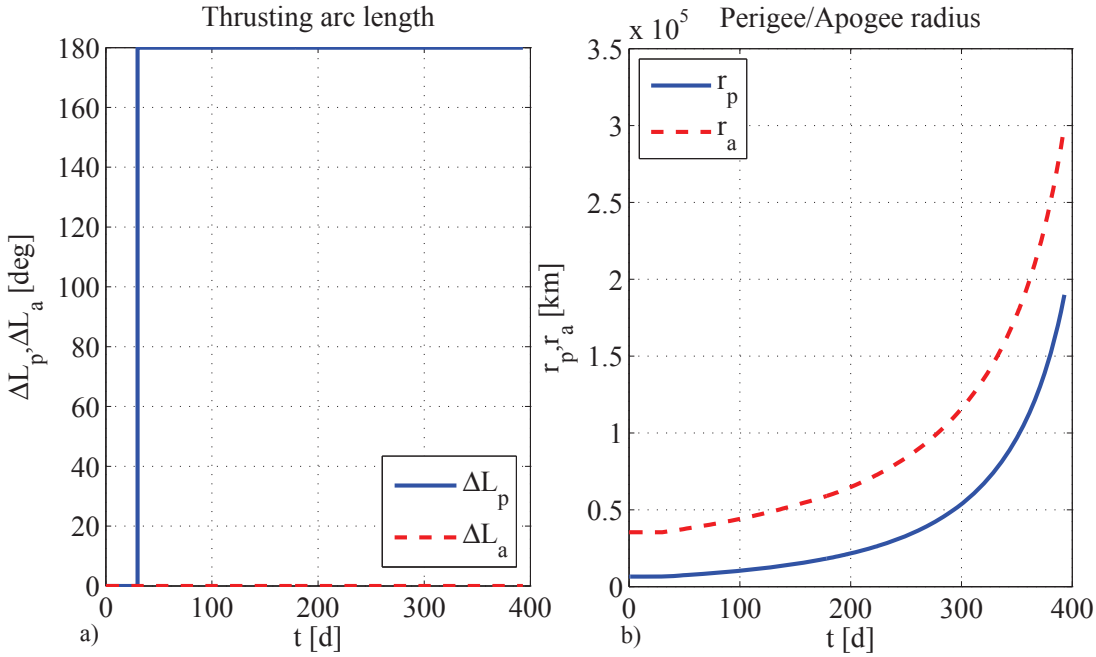

Figure 7. Minimum *ToF* solution: a) thrusting arc length; b) perigee/apogee radii.

From Figure 8, which plots the trajectory in the J2000 reference frame, one can also clearly appreciate that the typical shape of a continuous tangential thrust trajectory as the orbit shape gradually becomes less eccentric.

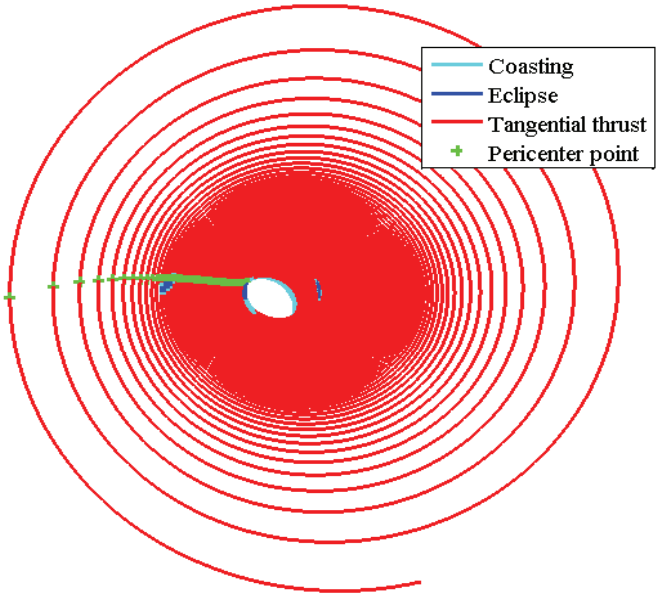

Figure 8. Minimum *ToF* solution: trajectory.

From Figure 9a, one can see that for the minimum *IES* solution, the thrusting arcs are located always around perigee with a semi-amplitude around 150-160 degrees. Consequently, the rate of increase of the orbit size is much lower (see Figure 9b) and at the same time the effort is focused on raising the apogee while the perigee experiences only a comparatively small increase up to around 30000 km, leading to the high t_{belt} mentioned before.

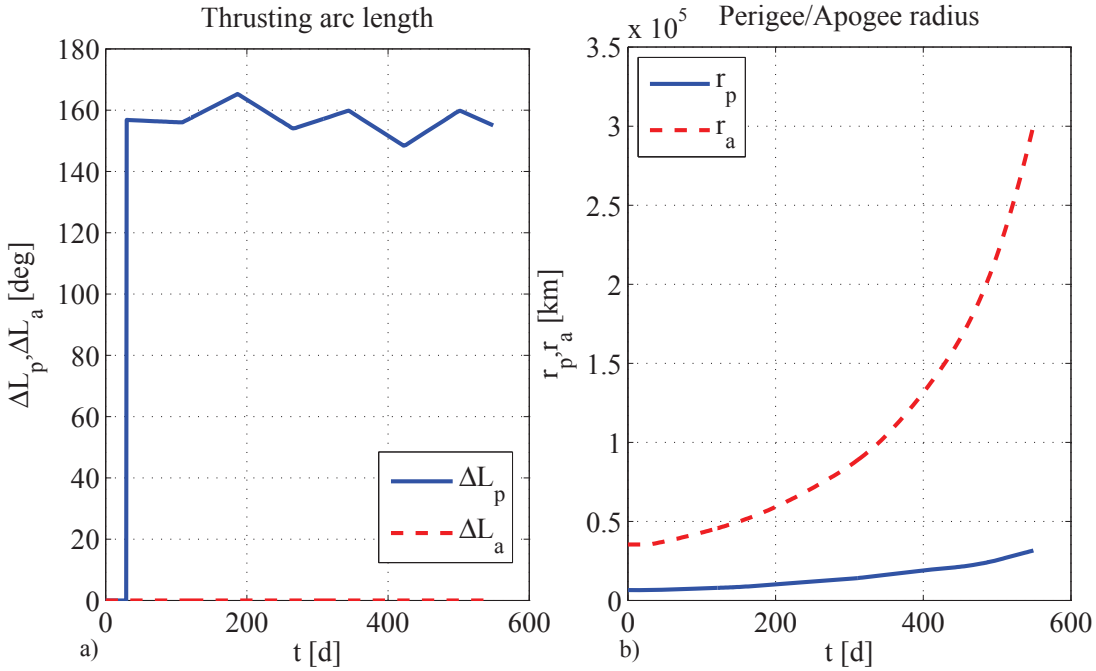

Figure 9. Minimum *IES* solution: a) thrusting arc length; b) perigee/apogee radii.

In contrast to the minimum *ToF* case, the long coasting arcs around apocenter lead to a considerable increase in the eccentricity, as shown in Figure 10.

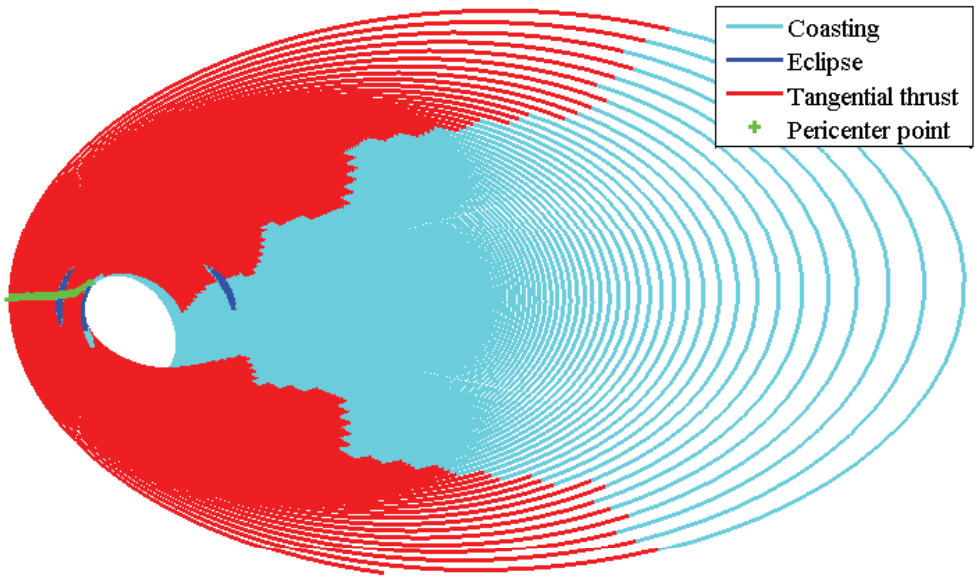

Figure 10. Minimum *IES* solution: trajectory.

The control strategy of the third case, as shown in Figure 11a, is a mix of the first two. In the first part, the thrust is continuous in order to raise the perigee above the radiation belt as soon as possible. After this has been achieved, at around 250 days, the length of the thrusting arcs is radically reduced in order to save propellant by concentrating on raising the apogee while keeping the perigee almost constant (see Figure 11b).

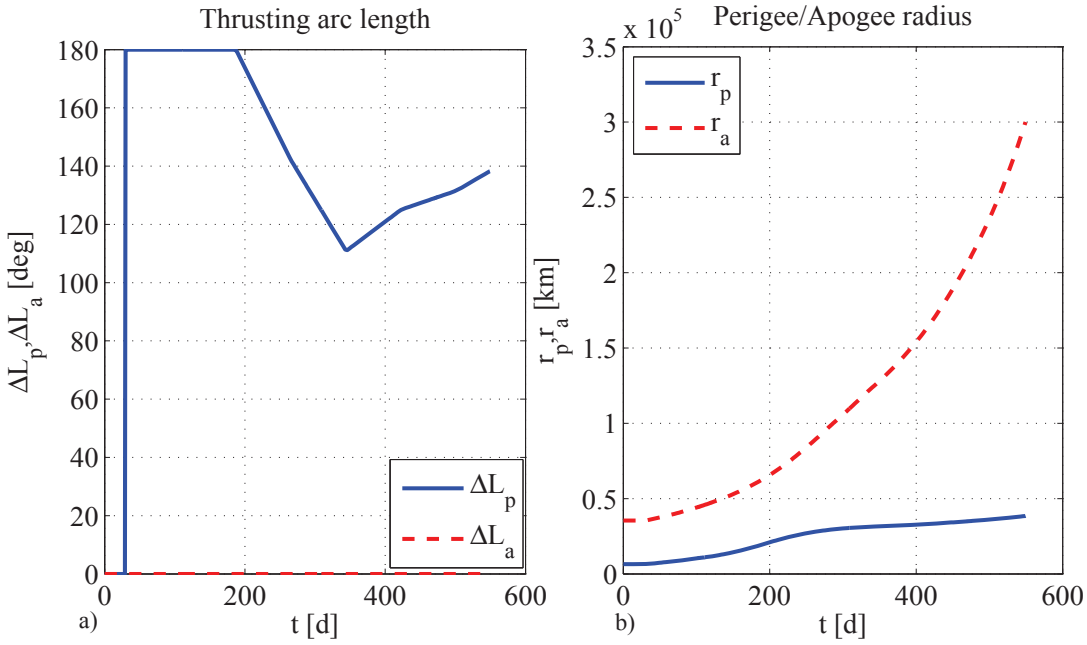

Figure 11. Minimum t_{belt} maximum *ToF* solution: a) thrusting arc length; b) perigee/apogee radii.

Figure 12 shows a view of the complete trajectory and clearly reveals the uninterrupted thrusting strategy in the initial part of the trajectory, followed by a phase with long coasting arcs around apocenter which lead to a gradual increase of the eccentricity, which is however lower than in the previous case.

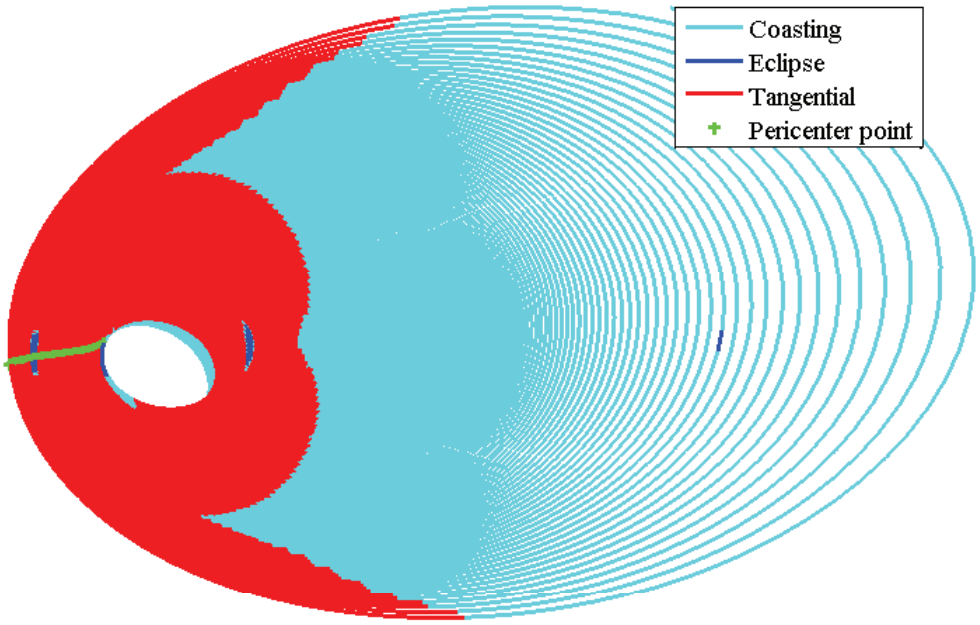

Figure 12. Minimum t_{belt}, maximum *ToF* solution:trajectory.

4-Objective problem

For the 4-objective case, MACS2 is run for a total of $6 \cdot 10^5$ function evaluations.

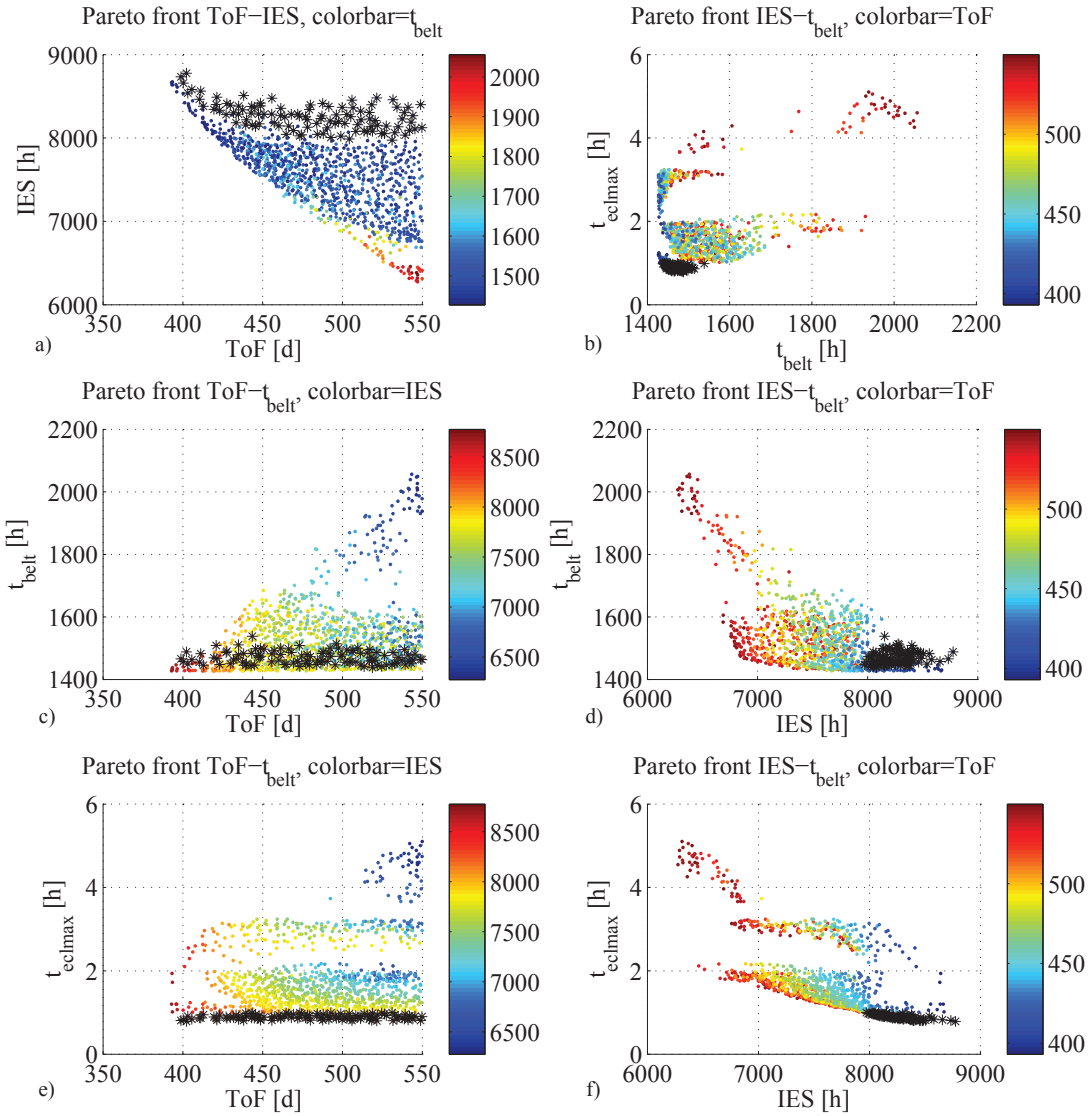

Figure 13. 4-Objective problem: Projections of the 4-dimensional Pareto set on the a) *ToF-IES* b) t_{belt}-$t_{ecl,max}$ c) *ToF*-t_{belt} d) *IES*-t_{belt} e) *ToF*-$t_{ecl,max}$ f) *IES*-$t_{ecl,max}$ sub-spaces. Black asterisks denote solutions with $t_{ecl,max} \leq 1$ h.

Figure 13 shows the set of the Pareto-optimal solutions, projected onto each of the bi-dimensional sub-spaces. Black asterisks denote the solutions which have the longest eclipse below 1 hour. In this respect, it is immediately apparent that there is no feasible solution with *IES* below 8000 hours (see Figure 13a). Similarly, from Figure 13b one can see that all these solutions have t_{belt} which is 1600 hours at most. This suggests that, in this case, solutions with a fast initial orbit raising phase are optimal for avoiding eclipses.

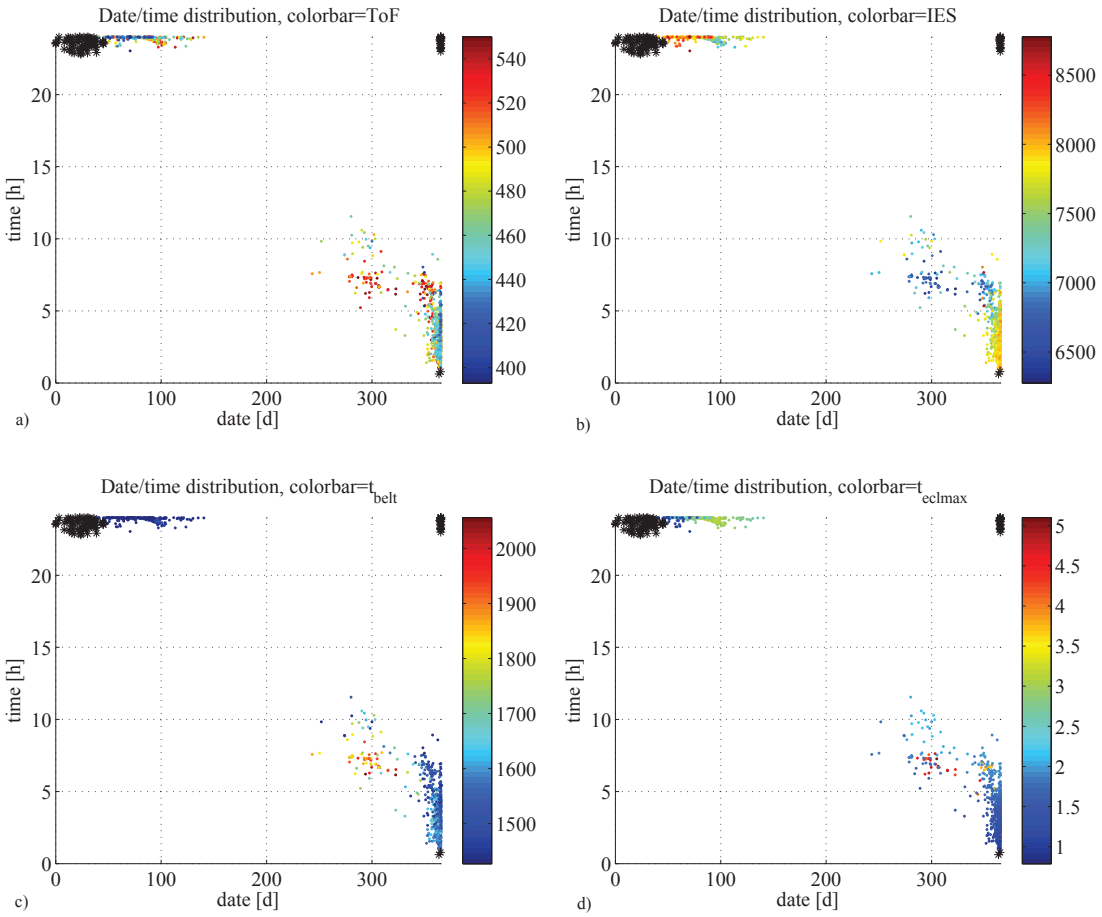

Figure 14. 4-Objective problem: distribution of the optimal solutions w.r.t. the departure date: a) *ToF* b) *IES* c) t_{belt} d) $t_{ecl,max}$. Black asterisks denote solutions with $t_{ecl,max} \leq 1$ h.

Figure 14 shows the distribution of the optimal solutions with respect to departure date and departure time. Generally speaking, their distribution is similar to that of the 3-objective case shown in Figure 6, as they are roughly aligned along a diagonal line. Solutions with a feasible eclipse, however, are restricted to a very small region around 24/0 h and 365/0 days, at the corners in Figure 14 (Note that, due to the annual periodicity of the Earth system, the regions at the four corners of the *date*/*time* plot, are by all practical means contiguous). This clearly shows that the introduction of the upper boundary on the maximum eclipse time is considerably limiting the launch opportunities and their performance, at least under the control model adopted. At the same time, however, it is important to consider that the solution of the Multi-Objective optimisation problem as formulated in (3) will return only the globally optimal solutions. This means that feasible, although inferior, solutions might still exist for other departure dates but, since they are dominated by other solutions, they are discarded during the optimisation process. On the other hand, at the preliminary design stage, it is desirable to investigate the existence of feasible solutions in less optimal regions of the launch window as well. This could also provide a good database of back-up solutions, should the optimal period for departure, as shown in Figure 14, become unfeasible due to other factors. A simple way to perform this kind of analysis would be to partition the parameter space (see Table 3) in a number of subsets along the *date* coordinate, and run separate Multi-Objective optimisation instances in each of them. However, this would require

as many optimisation instances as the partitions of the domain D and at the same time, the fact that they would run separately would prevent an exchange of information between each of them. Therefore, the following alternative has been adopted, which requires only a single MO instance, and which consists in modifying the 4-Objective problem in (3) by adding two *dummy* performance parameters to **f**, as:

$$\mathbf{f} = \left[ToF \quad IES \quad t_{belt} \quad t_{ecl,max} \quad \frac{date}{365} \quad 1 - \frac{date}{365} \right] \tag{6}$$

This modification makes such that a solution, even if it is inferior to another with regard to *ToF*, *IES*, t_{belt} or $t_{ecl,max}$, is still not discarded by the optimisation algorithm as long as its departure date is different from the other. Or, in other words, the optimiser will automatically search for and store the optimal solutions, in terms of *ToF*, *IES*, t_{belt} or $t_{ecl,max}$, *for each departure date*. This modified 4-objective problem, formally a 6-objective one, is again solved with MACS2, with 10^6 function evaluations.

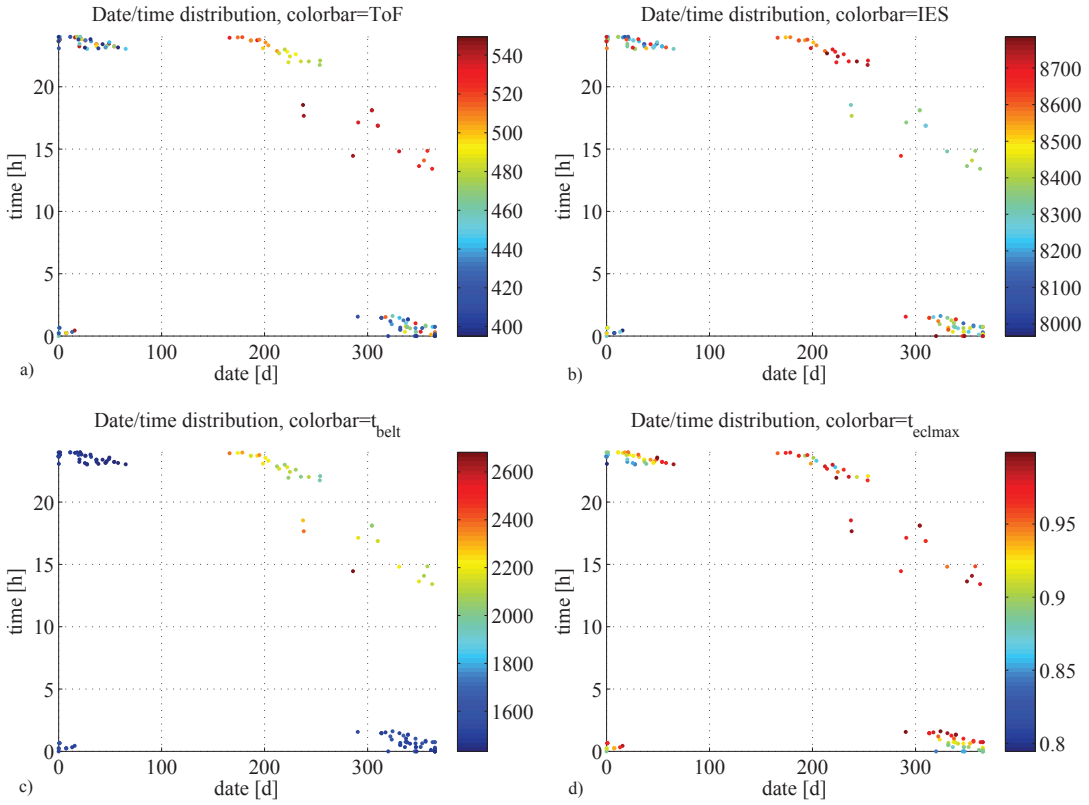

Figure 15. Modified 4-Objective problem: distribution of the optimal solutions with $t_{ecl,max} \leq 1$ h w.r.t. the departure date: a) *ToF* b) *IES* c) t_{belt} d) $t_{ecl,max}$.

Figure 15 shows the distribution of optimal solutions with maximum eclipse duration shorter than 1 hour and reveals the existence of two new clusters of solutions in addition to those already identified in the previous, 4-objective case. One lies in the summer period close to midnight time while the other is in autumn in the 15-20 h range. Although they differ slightly in terms of performance parameters, a number of considerations apply to both groups. First, they both have a higher time of flight than the winter/midnight class, ranging from 480 to 550 days. At the same time, their propellant cost is also quite high, as is t_{belt}, which is between 2000 and 2600 hours. As

an example, Table 5 reports the relevant parameters for a typical solution in this group, which can be compared to those in Table 4. Figure 16 plots its thrusting arc length and time history of perigee and apogee radii.

Table 5. Sample solution in Summer with feasible eclipse.

date (d)	*time* (h)	*ToF* (d)	*IES* (h)	t_{belt} (h)	$t_{ecl,max}$ (h)
198	23.3	498	8581	2140	0.92

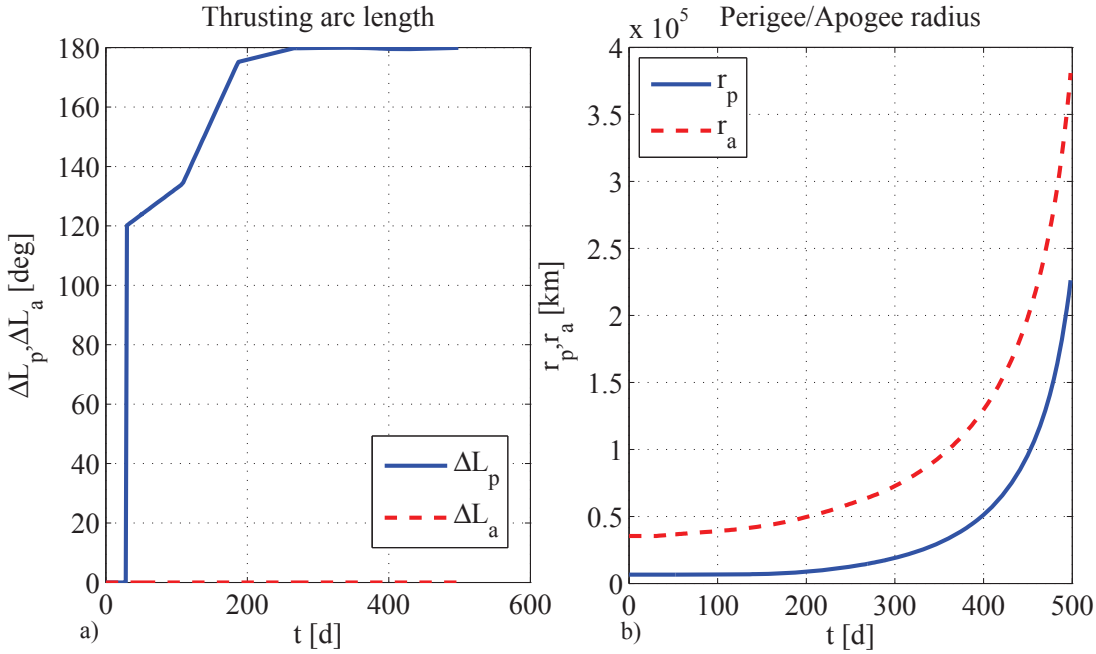

Figure 16. Summer solution with feasible eclipse: a) thrusting arc length; b) perigee/apogee radii.

As Figure 16a shows, at the beginning, the thrusting arcs are located around perigee with a semi-amplitude of 120 degrees, which then progressively increases to 180 degrees (i.e. continuous thrust) at 250 days. This might seem quite odd at first since it has the obvious drawback of increasing both the total transfer time and the exposure to the environment of the radiation belts, as testified by Table 5. Moreover, the relative geometry between the spacecraft's orbit and the lunar one is far from optimal because, as can be seen in Figure 16b, the final apogee is well above 300000km, which means that the intersection with the lunar orbit plane is far from the line of apses. On the other hand, it is important to keep in mind that the driving factor for which this candidate solution has been selected is its low maximum eclipse duration. In this sense, the control profile is meant at altering the geometry relative geometry between DESTINY's orbit and the shadow region in order to minimise eclipse duration. While a more detailed discussion of the specific issues of eclipses during DESTINY's orbit raising and related avoidance techniques will be the topic of a future work, it is still important to introduce here a number of observations. First, one has to consider that, due to the relatively high inclination of DESTINY's orbit with respect to the Ecliptic, and due to the periodicity of the apparent motion of the Sun around the Earth, the shadow region will intersect the orbit plane at more or less regular intervals. Therefore, eclipses are typically encountered in a number of separate phases. In other words, there will be parts of the

transfer in which there is one eclipse per orbit, separated by phases in which there are no eclipses at all.

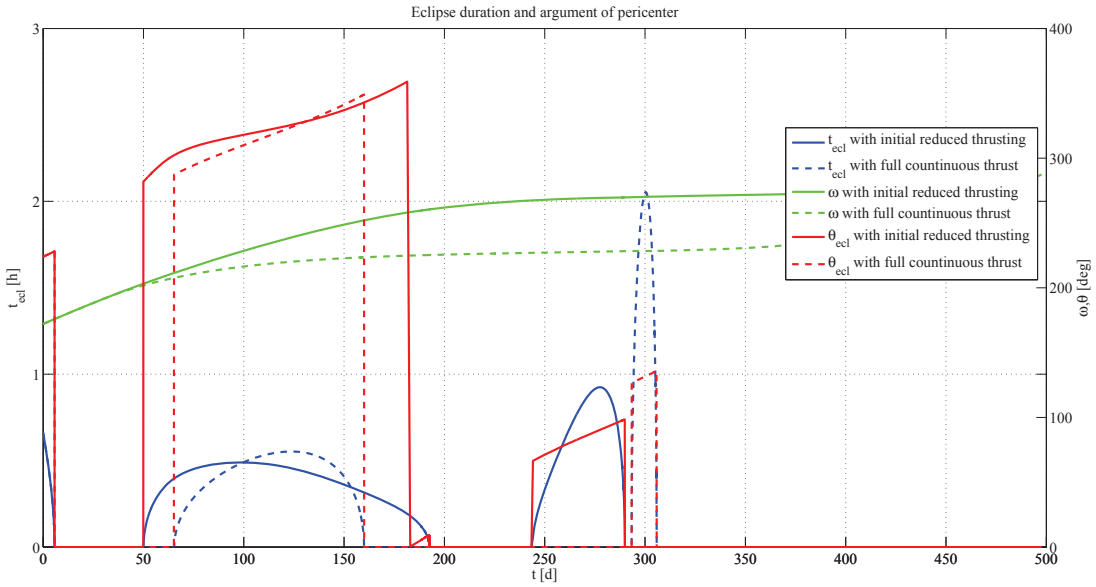

Figure 17. Eclipse duration, argument of pericenter and true anomaly of shadow region for two sample solutions.

A visualisation of this can be found in Figure 17, which shows the time history of three important quantities: the duration of each single eclipse t_{ecl} (blue line), the argument of perigee ω in the ecliptic reference frame (green line) and finally the true anomaly of the axis of the shadow region θ_{ecl} on the orbit plane (red line). The continuous line refers to the case of the solution in Table 5, while the dashed line refers to a trajectory with same departure epoch as the previous one, but with a simple continuous thrust profile as the one shown in Figure 7. As mentioned before, one can recognise three different eclipse phases: a very short one during the commissioning phase, a relatively long one between 50 and 180 days and a shorter one between 240 and 290 days. In the case of the trajectory with reduced thrusting, in none of these three phases the duration of a single eclipse exceeds one hour, making this a feasible trajectory. On the contrary, for the continuous thrust case, in the third sequence of eclipses there is a peak of 2 hours duration. One can seek an explanation for this fundamental difference by examining the time history of θ_{ecl} (the true anomaly of the axis of the shadow region) in each case. Given the ellipticity of DESTINY's orbit, this parameter becomes very important since, the closer to the apocenter the shadow region is, the longer is the time the spacecraft will need to cross it. In the first case, θ_{ecl} is around 90 degrees, which means that the shadow region lies much closer to the pericenter than the apocenter. In the second case, θ_{ecl} is around 130 degrees, i.e. closer to the apocenter and this is the main reason for which eclipses are longer in this case. The cause for the different position of the shadow in the two cases is found if one checks the behaviour of the argument of pericenter: in both cases there is an asymptotic increase of ω with time. However, in the cases with full continuous thrust the transient phase ends earlier and the total variation of ω is some 40 degrees smaller than in the other case, leading to the critical eclipse at 300 days. This variation of ω is essentially due to the J_2 effect. In this sense, while the continuous thrust solution experiences this perturbation for less since it raises the orbit very quickly, the solution with initial reduced thrust spends more time in proximity of the Earth and therefore the J_2 effect acts for longer and leads to a larger rotation of the line of apses. As a side note, note also that, in this case, the second eclipse phase

lasts longer and the third one is encountered at an earlier date than in the continuous thrust case. Without entering into too much detail, this is due to the fact the rotation of the line of nodes of the orbit is different in the two cases, again due to the different action of the J_2 perturbation.

In summary, it can be said that this solution is exploiting the J_2 perturbation to passively rotate the line of apses and obtain a favourable relative geometry with the shadow region in order to avoid long eclipses. In order to obtain this, of course, it sacrifices time of flight and transit time in the radiation belt and consequently it is not a globally optimal transfer but nevertheless it constitutes a feasible alternative if a departure date in seasons other than winter becomes imperative.

CONCLUSIONS

This paper presented the preliminary design of the initial, Low-Thrust orbit raising phase for DESTINY mission. Multiple design drivers and constraints were taken into account by formulating the design problem as a Multi-Objective optimisation problem. The high computational cost and number of parameters related to Low-Thrust trajectory design was overcome by adopting an averaged analytical propagation technique and by using a simplified control parameterisation. The MO problem was solved by means of a stochastic global optimisation algorithm. The results obtained provided a good picture of the different transfer options and their inherent trade-offs. At the same time, detailed analysis of the results allowed for a better understanding of the dynamics of the orbit raising problem. In particular, the constraint on maximum eclipse duration was shown to be a very critical requirement, which restricts the optimal departure opportunities to the winter/midnight range. However, if sub-optimal solutions are also considered, transfer opportunities are available for 75% of the year, albeit with a high transit time within the radiation belts. Analysis of some of these solutions also suggested possible control strategies aimed specifically at avoiding long eclipses, and these will be the topic of a future work.

REFERENCES

[1] Kawakatsu, Y. and Iwata, T.: DESTINY Mission Overview - A Small Satellite Mission for Deep Space Exploration Technology Demonstration, The 13th International Space Conference of Pacific-basin Societies, 2012.

[2] Vasile, M. and Zuiani, F.: Multi-agent collaborative search: an agent-based memetic multi-objective optimization algorithm applied to space trajectory design, Proceedings of the Institution of Mechanical Engineers, Part G: Journal of Aerospace Engineering, 2011.

[3] Kechichian, J.A.: Low-Thrust Eccentricity-Constrained Orbit Raising, Journal of Spacecraft and Rockets, Vol. 35, 327-335, 1998.

[4] Kechichian, J.A.: Orbit Raising with Low-Thrust Tangential Acceleration in Presence of Earth Shadow, Journal of Spacecraft and Rockets, Vol. 35, 516-525, 1998.

[5] Casalino, L. and Colasurdo, G.: Improved Edelbaum's Approach to Optimize Low Earth/Geostationary Orbits Low-thrust Transfers, Journal of Guidance, Control, and Dynamics, Vol. 30, Nr. 5, 1504-1510, 2007.

[6] Kluever, C.A. and Oleson, S.R.: Direct approach for computing near-optimal low-thrust earth-orbit transfers, Journal of Spacecraft and Rockets, Vol. 35, No. 4, 509-515, AIAA, 1998.

[7] Gao, Y. and Li, X.: Optimization of low-thrust many-revolution transfers and Lyapunov-based guidance, Acta Astronautica, Vol. 66, No. 1, 117-129, Elsevier, 2010.

[8] Zuiani, F., Vasile, M., Palmas, A. and Avanzini, G.: Direct transcription of low-thrust trajectories with finite trajectory elements, Acta Astronautica, Vol.72, 108-120, Elsevier 2012.

[9] Zuiani, F. and Vasile, M.: Extension of Finite Perturbative Elements for Multi-Revolution, Low-Thrust propulsion transfer optimisation, 63th International Astronautical Congress (IAC2012), IAC-12-C.1.4.6, Naples, October 1st-5th, 2012.

[10] Zuiani, F. and Vasile, M.: Extended Analytical Formulas for Low-Thrust Trajectory Design, Celestial Mechanics and Dynamical Astronomy, 2013 (Submitted).

[11] Zuiani, F. and Vasile, M.: Preliminary design of Debris removal missions by means of simplified models for Low-Thrust, many-revolution transfers, International Journal of Aerospace Engineering, Hindawi 2012.

[12] Escobal, P.: Methods of Orbit Determination, New York, John Wiley and Sons, 1965.

[13] Vallado, D.A.: Fundamentals of Astrodynamics and Applications, 3rd edition, Space Technology Library, Springer, 2007.

[14] Zuiani, F. and Vasile, M.: Multi-Agent Collaborative Search with Tchebycheff decomposition and Monotonic Basin Hopping steps, BIOMA2012, Bohinij, Slovenia, 2012.

[15] Zuiani, F. and Vasile, M.: Multi-Agent Collaborative Search based on Tchebycheff decomposition, Computational Optimisation and Applications, Accepted, 2013.